Supplement of Atmos. Chem. Phys., 25, 5773–5792, 2025
https://doi.org/10.5194/acp-25-5773-2025-supplement

Atmospheric Chemistry and Physics Open Access

Supplement of

Implications of reduced-complexity aerosol thermodynamics on organic aerosol mass concentration and composition over North America

Camilo Serrano Damha et al.

Correspondence to: Camilo Serrano Damha (camilo.serranodamha@mail.mcgill.ca) and Andreas Zuend (andreas.zuend@mcgill.ca)

Table of Contents

S1 Organic Aerosol Scheme in GEOS-Chem

S2 Implementation of the BAT-VBS model in GEOS-Chem

S3 Comparison between Water-Sensitive and Dry OA Schemes at Dry Conditions

S4 Organic Mass Concentration

S5 Mass Fractions of OA Compound Classes

S6 Sensitivity of Predicted Organic Mass Concentration to Assigned O:C

S7 Diurnal Cycle of OA

S8 Vertical Profile of OA

S9 Observations of Daily Mean $PM_{2.5}$ Mass Concentrations

S10 RH Threshold for the BAT-VBS model

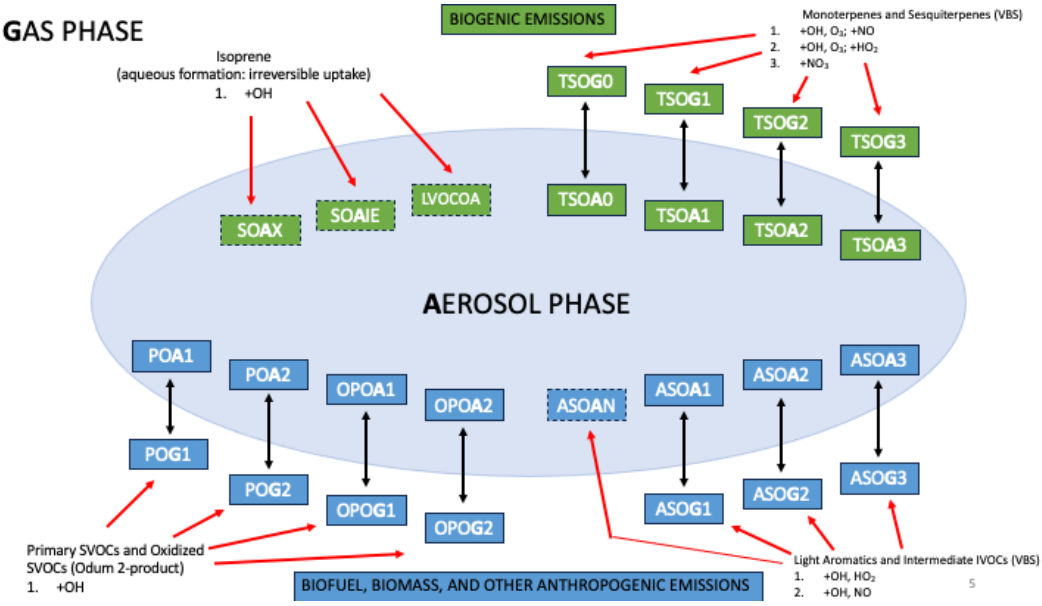

Figure S1. Schematic of all the OA species considered in the GEOS-Chem model (adapted from Fig. 1 in Pye et al. (2010)). OA species are in boxes. Dashed boxes and unidirectional red arrows across the aerosol/gas interface indicate OA species that do not partition to the gas phase. Solid boxes and bidirectional black arrows across the aerosol/gas interface indicate OA species that can partition between the gas phase and the particle phase. Green boxes represent OA species from biogenic sources. Blue boxes represent OA species from anthropogenic sources. As described in Pye et al. (2010), the gas–particle partitioning is parameterized with either a unique 1D VBS with four C_j^* bins, in the case of TSOA and ASOA, or an Odum 2-product fit with two C_j^* bins, in the case of POA and OPOA. Isoprene-derived OA is modeled using an aqueous phase irreversible reactive uptake scheme by Marais et al. (2016). The OA species from terpenes are TSOA0 ($C_j^* = 0.1\ \mu g\ m^{-3}$), TSOA1 ($C_j^* = 1\ \mu g\ m^{-3}$), TSOA2 ($C_j^* = 10\ \mu g\ m^{-3}$), and TSOA3 ($C_j^* = 100\ \mu g\ m^{-3}$). The OA species from isoprene are SOAGX ($C_j^* = 0\ \mu g\ m^{-3}$), SOAIE ($C_j^* = 0\ \mu g\ m^{-3}$), and LVOCOA ($C_j^* = 0\ \mu g\ m^{-3}$). The OA species from light aromatics & intermediate-volatility organic compounds are ASOAN ($C_j^* = 0\ \mu g\ m^{-3}$), ASOA1 ($C_j^* = 1\ \mu g\ m^{-3}$), ASOA2 ($C_j^* = 10\ \mu g\ m^{-3}$), and ASOA3 ($C_j^* = 100\ \mu g\ m^{-3}$). The OA species from primary semivolatile organic compounds are POA1 ($C_j^* = 1646\ \mu g\ m^{-3}$) and POA2 ($C_j^* = 20\ \mu g\ m^{-3}$). the OA species from oxidized semivolatile organic compounds are OPOA1 ($C_j^* = 16.46\ \mu g\ m^{-3}$) and OPOA2 ($C_j^* = 0.2\ \mu g\ m^{-3}$). The reference T for C_j^* of TSOA and ASOA species is 298 K. The reference T for C_j^* of POA and OPOA species is 300 K.

S1 Organic Aerosol Scheme in GEOS-Chem

The OA species in this work are grouped together into five compound classes corresponding to five main hydrocarbon precursors: terpenes (TSOA/G), isoprene (ISOA/G), light aromatics and intermediate-volatility organic compounds (IVOCs) (ASOA/G), primary semivolatile organic compounds (SVOCs) (POA), and oxidized SVOCs (OPOA) (Pye et al., 2010). A schematic of all the OA species considered in GEOS-Chem is shown in Fig. S1. The properties of these species are summarized in Sec. 2.1.

S2 Implementation of the BAT-VBS model in GEOS-Chem

Our implementation of the BAT-VBS model in GEOS-Chem involved two main steps. First, the molecular properties of organic surrogate species required by the BAT-VBS model had to be estimated, as described in Sec. 2.1. Second, the equations of GEOS-Chem's default OA partitioning scheme (complex secondary OA scheme with semivolatile primary OA) were replaced by the BAT-VBS model.

Gas-phase reactions take place between oxidants (e.g., O_3 or OH, NO, HO_2, NO_3 radicals) and OA precursors (e.g., terpenes, isoprene, light aromatics, intermediate-volatility organic compounds, primary semivolatile organic compounds, and oxidized semivolatile organic compounds) in each grid cell and time step of the GEOS-Chem model. The organic oxidation products distribute their mass between the gas phase and the aerosol phase. To achieve equilibrium and estimate the aerosol mass fraction (AMF) of each oxidation product, the default OA scheme of the GEOS-Chem model solves an implicit equation for the total OA organic mass concentration, which only contains dry organic mass (i.e., without considering the OA water uptake). In our simulations, the GEOS-Chem model considers primary and secondary OA species as semivolatile. The equation to solve, derived from absorptive gas–particle partitioning theory (i.e., vapor–liquid equilibrium) (Pankow, 1994, 2003; Donahue et al., 2006; Zuend et al., 2010) and mass balance on each oxidation product, is:

$$\frac{\sum_j \left(C_j^{\mathrm{gas}} + C_j^{\mathrm{SV\,OA}}\right)}{C_j^* \left(1 + \frac{C_{org}^{\mathrm{OA}}}{C_j^*}\right)} = 1, \tag{S1}$$

where $C_j^{\mathrm{SV\,OA}}$ is the OA organic mass concentration, C_j^{g} is the gas-phase organic mass concentration, and C_j^* is the gas–particle partitioning coefficient, also known as the effective saturation mass concentration, of each semivolatile species j. $C_{org}^{\mathrm{OA}} = \sum_j C_j^{\mathrm{SV\,OA}}$ is the total OA organic mass concentration. The VBS solver determines C_{org}^{OA} implicitly from Eq. (S1) by varying its value until convergence is achieved.

The implicit equation for $C_{org}^{\mathrm{SV\,OA}}$ (Eq. S1) has a solution only when (Chung and Seinfeld, 2002):

$$\sum_j \frac{C_j^{\mathrm{SV\,OA}} + C_j^{\mathrm{gas}}}{C_j^*} > 1, \tag{S2}$$

where C_j^{g} is the gas-phase mass concentration of each organic component j. Once C_{org}^{OA} is calculated implicitly from Eq. (S1), the aerosol mass fraction (AMF) of each organic component j can be determined, assuming constant, RH-independent C_j^* values, from:

$$\xi_j = \left(1 + \frac{C_j^*}{C_{org}^{\mathrm{OA}}}\right)^{-1}, \tag{S3}$$

where ξ_j is the AMF of each organic species j. In turn, the OA organic mass concentration of each organic species j is then determined by:

$$C_j^{\mathrm{SV\,OA}} = \xi_j \times C_j^{\mathrm{gas+SV\,OA}}, \tag{S4}$$

where $C_j^{\mathrm{gas+SV\,OA}}$ is the total (gas-phase plus particle-phase) mass concentration of organic species j.

The implementation of the BAT-VBS model into GEOS-Chem increases the number of independent variables since C_j^* values are no longer constant for a given T. They are then also a function of OA water content (or, indirectly, RH). Water uptake alters the particle-phase mole fractions and mole-fraction-based activity coefficients of organic species j, in addition to the mass-concentration-weighted harmonic mean molar mass of OA (Serrano Damha et al., 2024). As a result, the procedure described through Eqs. (S1)–(S3) needs to be modified as convergence cannot be achieved only by iterating over C_{org}^{OA} since C_j^* cannot be considered constant. Instead, the BAT-VBS model solves a system of coupled algebraic equations numerically by iterating over ξ_j (Gorkowski et al., 2019). This means that updated values for C_{org+w}^{OA} (Eq. 3) and C_j^* (Eq. (2) are calculated during every VBS solver iteration step until ξ_j converges, slightly increasing the computational cost of a nonideal VBS approach in comparison to the standard (dry) VBS of GEOS-Chem.

S3 Comparison between Water-Sensitive and Dry OA Schemes at Dry Conditions

The water-sensitive (introduced) and dry (default of GEOS-Chem) OA partitioning schemes were compared at dry conditions (RH = 0 %) by running the GEOS-Chem model over North America for July and January 2019. The default partitioning scheme of GEOS-Chem corresponds to the unmodified secondary OA scheme that accounts for semivolatile primary OA, which is inherently dry. The introduced water-sensitive OA scheme (BAT-VBS model) was forced to run at RH = 0 %. The absolute and relative differences in mean OA organic mass concentrations over the North American subdomain, averaged over the 72 vertical levels and 248 time steps (3-hourly data for 31 days), are shown in Fig. S2. The absolute and relative differences in mean surface OA organic mass concentrations are shown in Fig. S3. The temporal average in Fig. S3 is restricted to the surface level only. The dry (default of GEOS-Chem) OA scheme is used as the reference to calculate the differences between OA partitioning schemes. The absolute differences in mean OA organic mass concentrations between the two OA partitioning schemes at dry conditions (RH = 0 %) are negligible. The highest relative differences in mean OA organic mass concentrations between the two OA partitioning schemes at dry conditions (RH = 0 %) are encountered in grid cells where the OA organic mass concentrations are extremely low (e.g., over the ocean). In those particular grid cells in which the default OA scheme of GEOS-Chem predicts very low OA organic concentrations, any divergence between the two OA schemes at dry conditions leads to high relative difference values.

These comparison results at dry conditions serve as a validation point for our implementation, since the water-sensitive OA scheme at dry conditions should predict the same OA organic mass concentration as GEOS-Chem's default (dry) OA scheme. The absolute and relative differences in OA organic mass concentration are attributed to the different OA partitioning solvers and tolerances used by the two OA partitioning schemes. To estimate more accurately the enhancement of OA organic mass concentration induced by the water-sensitive OA partitioning scheme, we decided to use the BAT-VBS model at dry conditions (RH = 0 %) as the OA partitioning scheme of reference in our results.

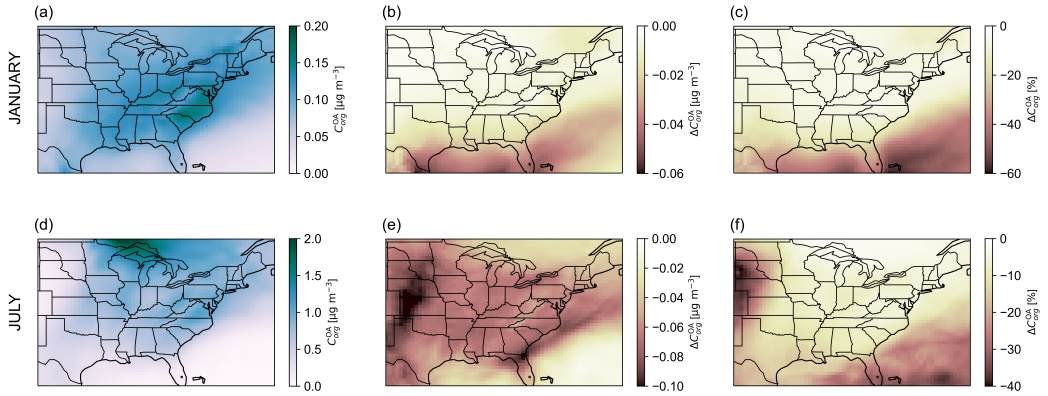

Figure S2. Comparison between GEOS-Chem's default (dry) and water-sensitive (BAT-VBS model) OA schemes in terms of predicted mean OA organic mass concentration at dry conditions (RH = 0 %) for January and July 2019. The mean is calculated over the 72 vertical levels (0.058 km to 78.146 km) and 248 time steps (3-hourly data for 31 days) of the GEOS-Chem nested simulation. Panels **(a)** and **(d)** show the mean OA organic mass concentration predicted by the introduced water-sensitive OA scheme (BAT-VBS model) when (forced to) run at RH = 0 %. Panels **(b)** and **(e)** show the (small) absolute difference in mean OA organic mass concentrations. Panels **(c)** and **(f)** show the relative difference in mean OA organic mass concentrations. The absolute and relative differences are calculated using the default (dry) OA scheme of GEOS-Chem as the reference ($C^{\mathrm{OA}}_{org,\mathrm{BAT-VBS}}$ (RH = 0 %)) - $C^{\mathrm{OA}}_{org,\mathrm{dry}}$).

S4 Organic Mass Concentration

The monthly mean OA organic mass concentration predicted at the surface by the water-sensitive OA scheme (BAT-VBS model) is shown in Fig. S4 for January and July 2019 in the entire North American domain (10°N–70°N, 140°W–40°W). Figure 2 illustrates the same results in a region that is centered on the Southeastern United States.

S5 Mass Fractions of OA Compound Classes

The contribution of organic compounds from biogenic and anthropogenic sources to the OA is expressed as their mass fractions with respect to the OA organic mass concentration (f_{org}). The monthly mean mass fractions of organic species from biogenic and anthropogenic sources at the first atmospheric level (0.058 km) of GEOS-Chem is shown in Fig. S5 for January and July 2019. Organic species from biogenic sources include the terpenes (TSOA) and isoprene (ISOA) compound classes. Organic species from anthropogenic sources include light aromatics and intermediate-volatility organic compounds (ASOA), primary semivolatile organic compounds (POA), and oxidized semivolatile organic compounds (OPOA). Their contributions to the monthly mean OA organic mass concentration at the first atmospheric layer are shown in Fig. S6.

The water-sensitive (updated) OA scheme that was used in GEOS-Chem in this work captures the variation of the effective volatility of organic species (C^*_j) with RH, a feature that GEOS-Chem's default (dry) OA scheme is missing. At RH > 0 %

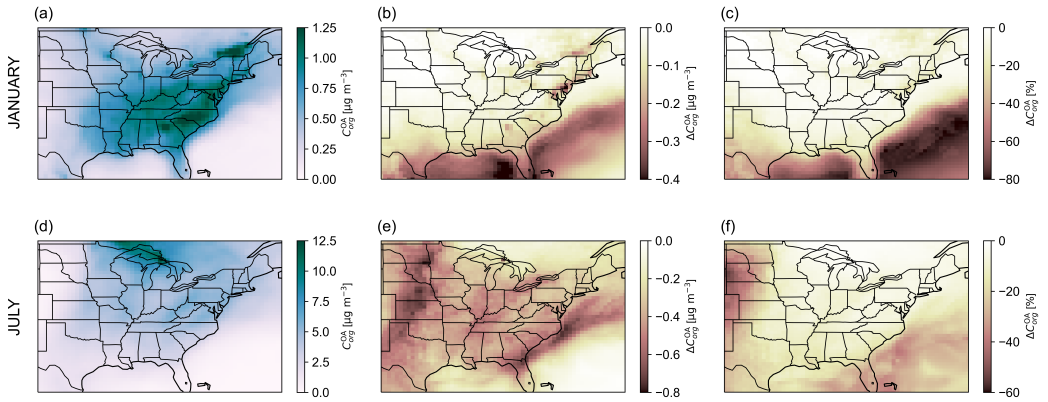

Figure S3. A comparison similar to Fig. S2, but restricted to the surface level. The surface mean is calculated over the 248 time steps (3-hourly data for 31 days) of the GEOS-Chem nested simulation. The surface level is the lowest atmospheric level of the GEOS-Chem model. Panels **(a)** and **(d)** show the mean OA organic mass concentration predicted by the introduced water-sensitive OA scheme (BAT-VBS model) when run at RH = 0 %. Panels **(b)** and **(e)** show the (small) absolute difference in mean OA organic mass concentrations. Panels **(c)** and **(f)** show the relative difference in mean OA organic mass concentrations. The absolute and relative differences are calculated using the default (dry) OA scheme of GEOS-Chem as the reference ($C^{\mathrm{OA}}_{org,\mathrm{BAT-VBS}}$ (RH = 0 %)) - $C^{\mathrm{OA}}_{org,\mathrm{dry}}$).

conditions, the water-sensitive OA scheme predicts lower C_j^* values than at dry conditions, and thus more OA organic mass concentration than the dry OA scheme (Fig. 2c, f). The individual contributions of organic compounds to the enhancement of OA organic mass concentration (when using the water-sensitive scheme instead of the dry scheme) are expressed as the ratio of their individual absolute difference in OA organic mass concentration and the cumulative absolute difference in OA organic mass concentration ($f_{\Delta org}$) considering all compound classes. The monthly mean individual contributions of the TSOA, ISOA, ASOA, POA, and OPOA compound classes to the monthly mean cumulative OA organic mass concentration enhancement at the first atmospheric layer (0.058 km) are shown in Figs. S7–S11 for January and July 2019.

S6 Sensitivity of Predicted Organic Mass Concentration to Assigned O:C

The elemental oxygen-to-carbon ratio of organic species (O:C$_j$) is one of the most important input properties for our water-sensitive OA scheme because it is assumed to be proportional to the polarity of the organic molecules. The more polar and water-soluble organic molecules are, the more water they will attract to the particle phase, therefore triggering a substantial decrease in the effective saturation mass concentration of organic compounds and enhancement of OA organic mass concentration.

We performed four nested GEOS-Chem simulations using the BAT-VBS model to assess the sensitivity of the predicted OA organic mass concentration to the assigned molecular properties of organic species. OA organic mass concentration data were

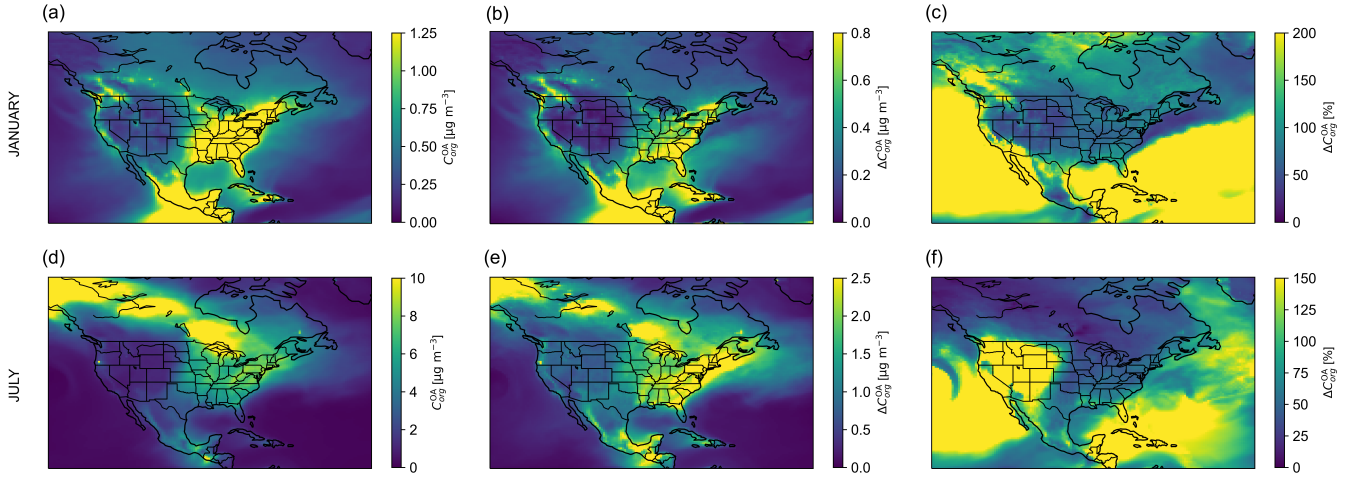

Figure S4. January 2019 (top panels) and July 2019 (bottom panels) **(a, d)** monthly mean surface OA organic mass concentration predicted by the introduced water-sensitive OA scheme (BAT-VBS model) at given RH in the entire North American domain (10°N–70°N, 140°W–40°W). Panels **(b)** and **(e)** show the absolute difference in monthly mean surface OA organic mass concentrations. Panels **(c)** and **(f)** show the relative difference in monthly mean surface OA organic mass concentrations. The surface level is the lowest atmospheric level of the GEOS-Chem model. The absolute and relative differences are calculated using the water-sensitive OA scheme (BAT-VBS model) at dry conditions as the reference ($C^{\mathrm{OA}}_{org,\mathrm{BAT-VBS}}$ (RH) - $C^{\mathrm{OA}}_{org,\mathrm{BAT-VBS}}$ (RH = 0 %)).

saved every 3 hours for the first week of July 2019. The same simulation setup described in Sec. 2.1 was employed, with the exception of using a 47-layer reduced vertical grid.

The four nested simulations included our introduced water-sensitive OA scheme. In the first simulation (A), the O:C$_j$ values were decreased by 30 % with respect to the values defined in Table 2. The molecular properties of simulation A are listed in Table S1. In the second simulation (B), the same O:C$_j$ values as defined in Table 2 were used. Simulation B applies our suggested molecular properties for organic species, which we used to produce the main results of this work. In the third simulation (C), O:C$_j$ values were increased by 30 % with respect to the values defined in Table 2. The molecular properties of simulation C are listed in Table S2. In simulations A and C, the molar masses of organic species (M_j) vary as a result of changing O:C$_j$ values according to the molecular corridor relationship discussed in Sec. 2.1. In the fourth simulation (D), the same O:C$_j$ values as defined in Table 2 were used, and RH was assumed to be equal to 0 %. Simulation D represents our baseline (dry) case against which the predicted OA organic mass concentrations from simulations A, B, and C are evaluated. Figure S12 shows the weekly mean surface OA organic mass concentration enhancement predicted by the introduced water-sensitive OA scheme (BAT-VBS model) for the first week of July 2019. The OA organic mass concentration enhancement is calculated in terms of absolute and relative differences with respect to the predictions of simulation D. The OA organic mass concentration enhancement increases with increasing O:C$_j$ values. The spatiotemporal mean enhancement in OA organic mass concentration is calculated over the area shown in Fig. S12 ($-105°$ to $-35°$ longitude and $25°$ to $50°$ latitude) and for

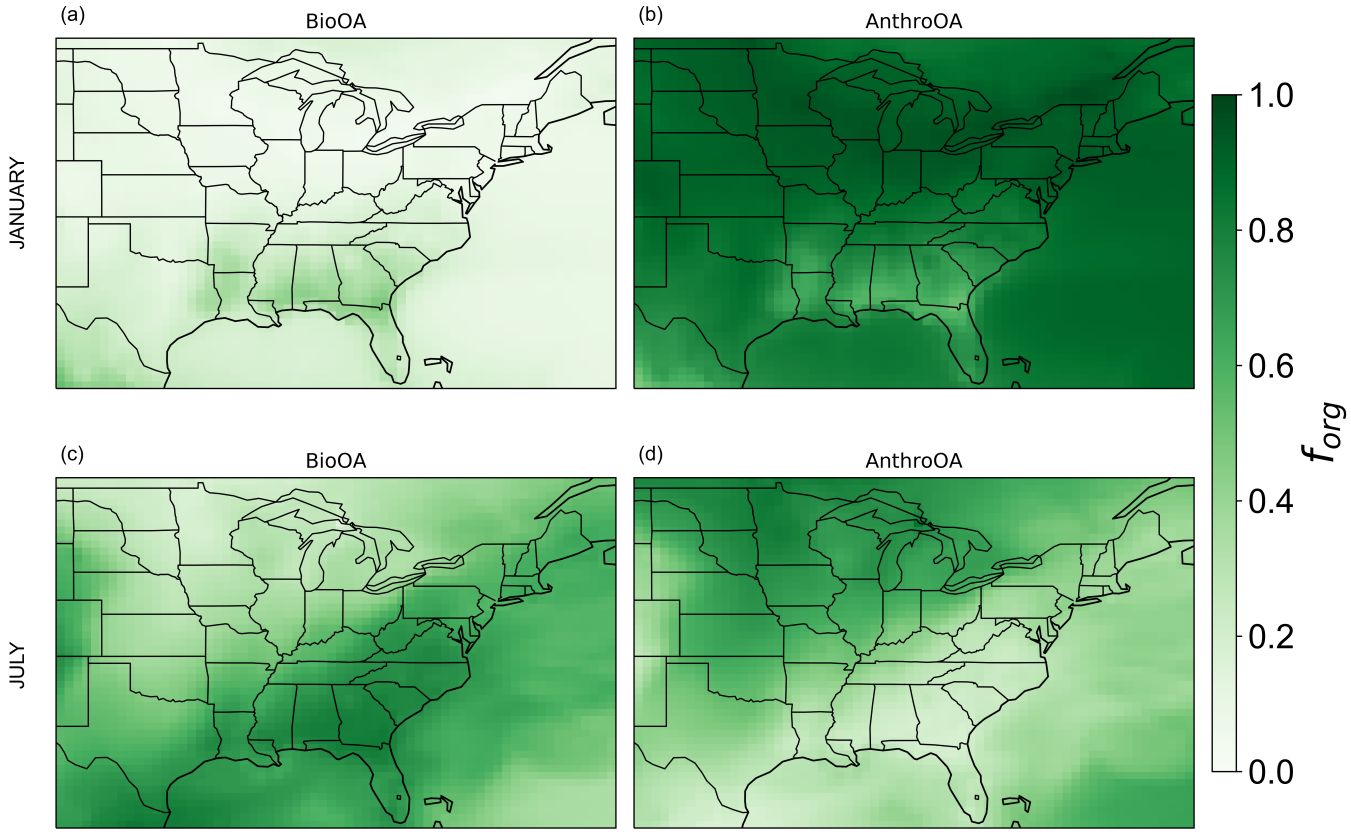

Figure S5. January 2019 (top panels) and July 2019 (bottom panels) monthly mean surface contribution of biogenic and anthropogenic OA species to the OA organic mass concentration, expressed as the organic mass fraction f_{org}. Panels **(a)** and **(c)** show the contribution from biogenic sources (BioOA). Panels **(b)** and **(d)** show the contribution from anthropogenic sources (AnthroOA).

the first week of July 2019. The mean absolute differences in OA organic mass concentration enhancement are $0.86\ \mu g\,m^{-3}$, $1.31\ \mu g\,m^{-3}$, and $1.45\ \mu g\,m^{-3}$ for simulations A, B, and C, respectively. The mean relative differences in OA organic mass concentration enhancement are $35.8\ \%$, $55.1\ \%$, and $61.3\ \%$ for simulations A, B, and C, respectively. An increase in polarity for organic species of lower O:C$_j$ triggers a more important OA organic mass concentration enhancement than an increase in polarity for organic species of higher O:C$_j$. Simulation A suggests a decrease in OA organic mass concentration enhancement of $34.3\ \%$ per $30\ \%$ decrease in O:C with respect to simulation B. Simulation C indicates an increase in OA organic mass concentration enhancement of $10.7\ \%$ per $30\ \%$ increase in O:C with respect to simulation B. Normalized on a per unit percent change of O:C, this means a sensitivity range of $0.36\ \%$ to $1.14\ \%$ in organic mass concentration enhancement per $1\ \%$ change in O:C of the organic compounds.

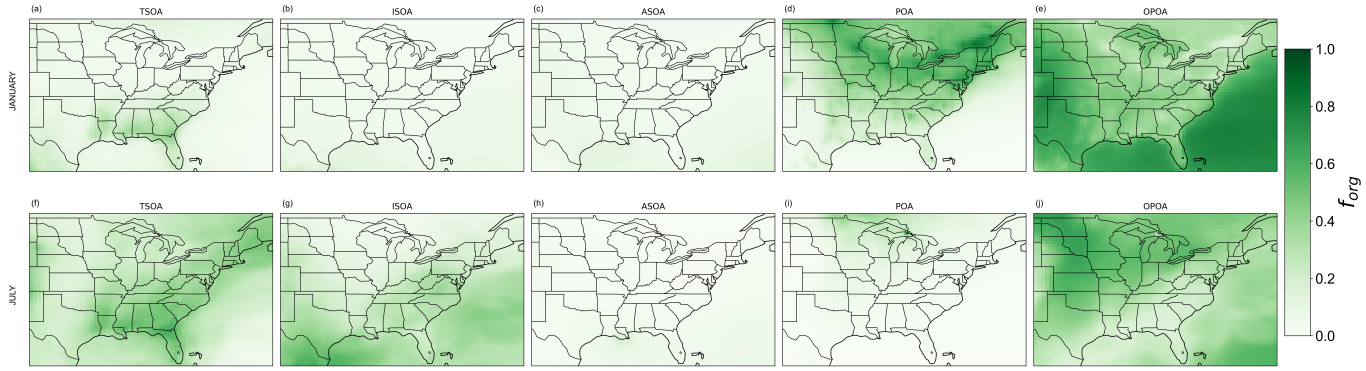

Figure S6. January 2019 (top panels) and July 2019 (bottom panels) monthly mean surface contribution of OA compound classes to the OA organic mass concentration, expressed as the organic mass fraction f_{org}. Panels **(a)** and **(f)** show the contribution of OA species from terpenes (TSOA). Panels **(b)** and **(g)** show the contribution of OA species from isoprene (ISOA). Panels **(c)** and **(h)** show the contribution of OA species from light aromatics & intermediate-volatility organic compounds (ASOA). Panels **(d)** and **(i)** show the contribution of OA species from primary semivolatile organic compounds (POA). Panels **(e)** and **(j)** show the contribution of OA species from oxidized semivolatile organic compounds (OPOA).

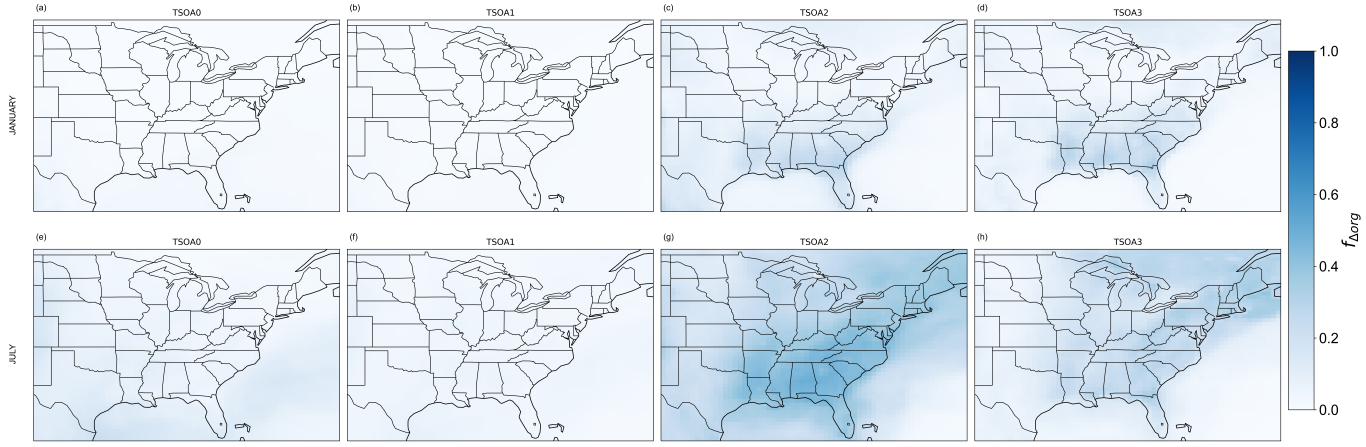

Figure S7. January 2019 (top panels) and July 2019 (bottom panels) monthly mean surface contribution of OA species from terpenes (TSOA) to the absolute difference in OA organic mass concentration, expressed as the organic mass concentration change fraction $f_{\Delta org}$. Panels **(a)** and **(e)** show the contribution of TSOA0 ($C_j^* = 0.1\ \mu g\,m^{-3}$). Panels **(b)** and **(f)** show the contribution of TSOA1 ($C_j^* = 1\ \mu g\,m^{-3}$). Panels **(c)** and **(g)** show the contribution of TSOA2 ($C_j^* = 10\ \mu g\,m^{-3}$). Panels **(d)** and **(h)** show the contribution of TSOA3 ($C_j^* = 100\ \mu g\,m^{-3}$).

S7 Diurnal Cycle of OA

Figure S13c shows the diurnal cycle of surface OA organic mass concentration for Montreal, Quebec, predicted by the water-sensitive (updated) and the dry OA schemes on July 3–4, 2019. The dry OA scheme corresponds to the introduced water-

Figure S8. January 2019 (top panels) and July 2019 (bottom panels) monthly mean surface contribution of OA species from isoprene (ISOA) to the absolute difference in OA organic mass concentration, expressed as the organic mass concentration change fraction $f_{\Delta org}$. Panels **(a)** and **(c)** show the contribution of SOAGX ($C_j^* = 0$ µg m^{-3}). Panels **(b)** and **(e)** show the contribution of SOAIE ($C_j^* = 0$ µg m^{-3}). Panels **(c)** and **(f)** show the contribution of LVOCOA ($C_j^* = 0$ µg m^{-3}).

sensitive OA scheme (BAT-VBS model) forced to run at RH = 0 %. As expected, RH increases from 8 p.m. to 8 a.m. local time the following day, at which point the maximum value is reached. RH then decreases until the cycle restarts in a similar fashion at 8 p.m. The diurnal cycle of atmospheric T follows almost the exact opposite pattern, where T decreases from 8 p.m. to 5 a.m. and reaches its lowest value at 5 a.m. T then increases until the cycle restarts at 8 p.m. The effective volatility of organic compounds typically decreases with decreasing T and increasing RH. The absolute (Fig. S13d) and relative (Fig. S13e) differences in OA organic mass concentrations are calculated using the dry OA scheme as the reference. Positive values mean that the water-sensitive OA scheme predicts a higher OA organic mass concentration than the dry OA scheme. The absolute and relative differences in OA organic mass concentrations closely follow the RH variation over the diurnal cycle: when RH increases (or decreases) with time, so does the difference between the two OA partitioning schemes. The diurnal cycle predicted by the dry OA scheme over Montreal varies due to T fluctuations and organic mass advection effects. Even though both OA schemes are exposed to the same T conditions and OA advection effects, the uptake of water and related feedback on the effective volatility of organic compounds that are accounted for by the water-sensitive scheme enhance the predicted OA organic mass concentration over the dry scheme. In this particular diurnal cycle, the water-sensitive OA organic mass concentration increases by more than 80 % at 8 a.m. with respect to the dry OA scheme when RH is at its maximum value.

Figure S9. January 2019 (top panels) and July 2019 (bottom panels) monthly mean surface contribution of OA species from light aromatics & intermediate-volatility organic compounds (ASOA) to the absolute difference in OA organic mass concentration, expressed as the organic mass concentration change fraction $f_{\Delta org}$. Panels **(a)** and **(e)** show the contribution of ASOAN ($C_j^* = 0$ µg m^{-3}). Panels **(b)** and **(f)** show the contribution of ASOA1 ($C_j^* = 1$ µg m^{-3}). Panels **(c)** and **(g)** show the contribution of ASOA2 ($C_j^* = 10$ µg m^{-3}). Panels **(d)** and **(h)** show the contribution of ASOA3 ($C_j^* = 100$ µg m^{-3}).

S8 Vertical Profile of OA

The hygroscopicity of OA is defined as its water affinity. The ability of OA to capture (and release) moisture from the environment is important for understanding cloud condensation nuclei (CCN) formation in the atmosphere. Petters and Kreidenweis (2007) introduced a relationship between the dry diameter of aerosol constituents and CCN activity. Typically, the hygroscopicity of OA is quantified in large-scale three-dimensional models with a simplified hygroscopicity parameter (κ) (Pankow and Barsanti, 2009; Zhang et al., 2012; Pankow et al., 2015; Jathar et al., 2016; Pye et al., 2017; Kim et al., 2019). This κ parameter relates the water captured by organic compounds in the OA to the composition dependence of the related binary solution water activity, which is equivalent to bulk equilibrium RH (Petters and Kreidenweis, 2007):

$$\frac{1}{a_{water}} = 1 + \kappa_{org}^{\mathrm{OA}} \frac{V_{org}^{\mathrm{OA}}}{V_{water}^{\mathrm{OA}}}, \tag{S5}$$

where a_{water} is the water activity of the aqueous OA solution, $\kappa_{org}^{\mathrm{OA}}$ is the hygroscopicity parameter of the OA, V_{org}^{OA} is the cumulative volume of water-free organic compounds in the OA, and V_{water}^{OA} is the volume of water taken up by organic compounds in the OA at a specified water activity level.

The cumulative volume V_{org}^{OA} can be calculated as the summation of the individual volumes of organic species j in the OA:

$$V_{org}^{\mathrm{OA}} = \sum_{n=1} V_j^{\mathrm{OA}}, \tag{S6}$$

where V_j^{OA} is the water-free volume of the organic compound j.

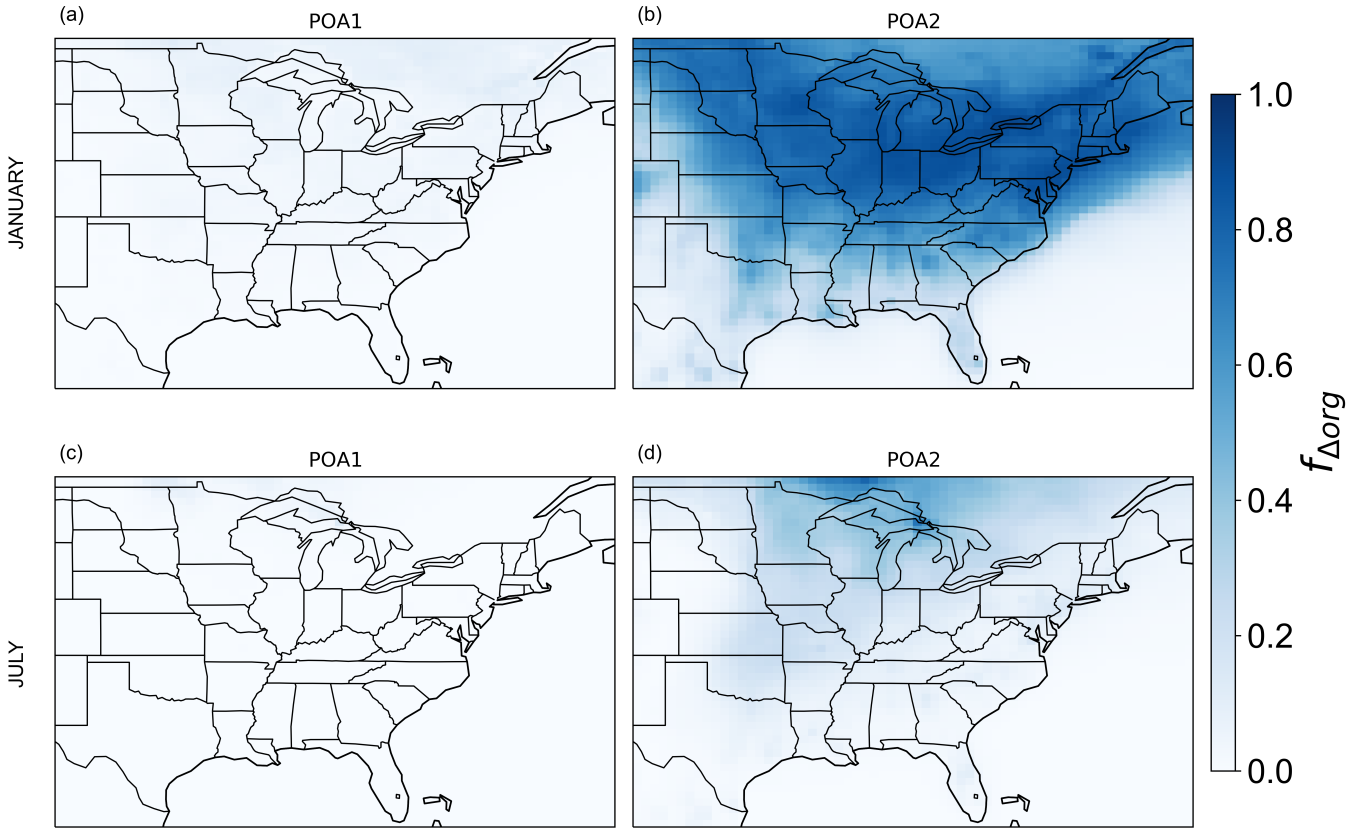

Figure S10. January 2019 (top panels) and July 2019 (bottom panels) monthly mean surface contribution of OA species from primary semivolatile organic compounds (POA) to the absolute difference in OA organic mass concentration, expressed as the organic mass concentration change fraction $f_{\Delta org}$. Panels **(a)** and **(c)** show the contribution of POA1 ($C_j^* = 1646\ \mu g\,m^{-3}$). Panels **(b)** and **(d)** show the contribution of POA2 ($C_j^* = 20\ \mu g\,m^{-3}$).

The cumulative volume V_{water}^{OA} is obtained from the equilibrium OA mass concentration of water due to all the organic species in the OA, which is an output of the BAT-VBS model:

$$V_{water}^{\mathrm{OA}} = \frac{C_{water}^{\mathrm{OA}}}{\rho_{water}^{\mathrm{OA}}}, \tag{S7}$$

where C_{water}^{OA} is the OA mass concentration of water that is taken up by all the organic species j in the OA and $\rho_{water}^{\mathrm{OA}}$ is the density of water.

The cumulative volume V_{org}^{OA} is obtained from the summation of the individual equilibrium OA organic mass concentrations of organic species in the OA, which are also outputs of the BAT-VBS model:

$$V_{org}^{\mathrm{OA}} = \sum_{n=1} \frac{C_j^{\mathrm{OA}}}{\rho_j^{\mathrm{OA}}}, \tag{S8}$$

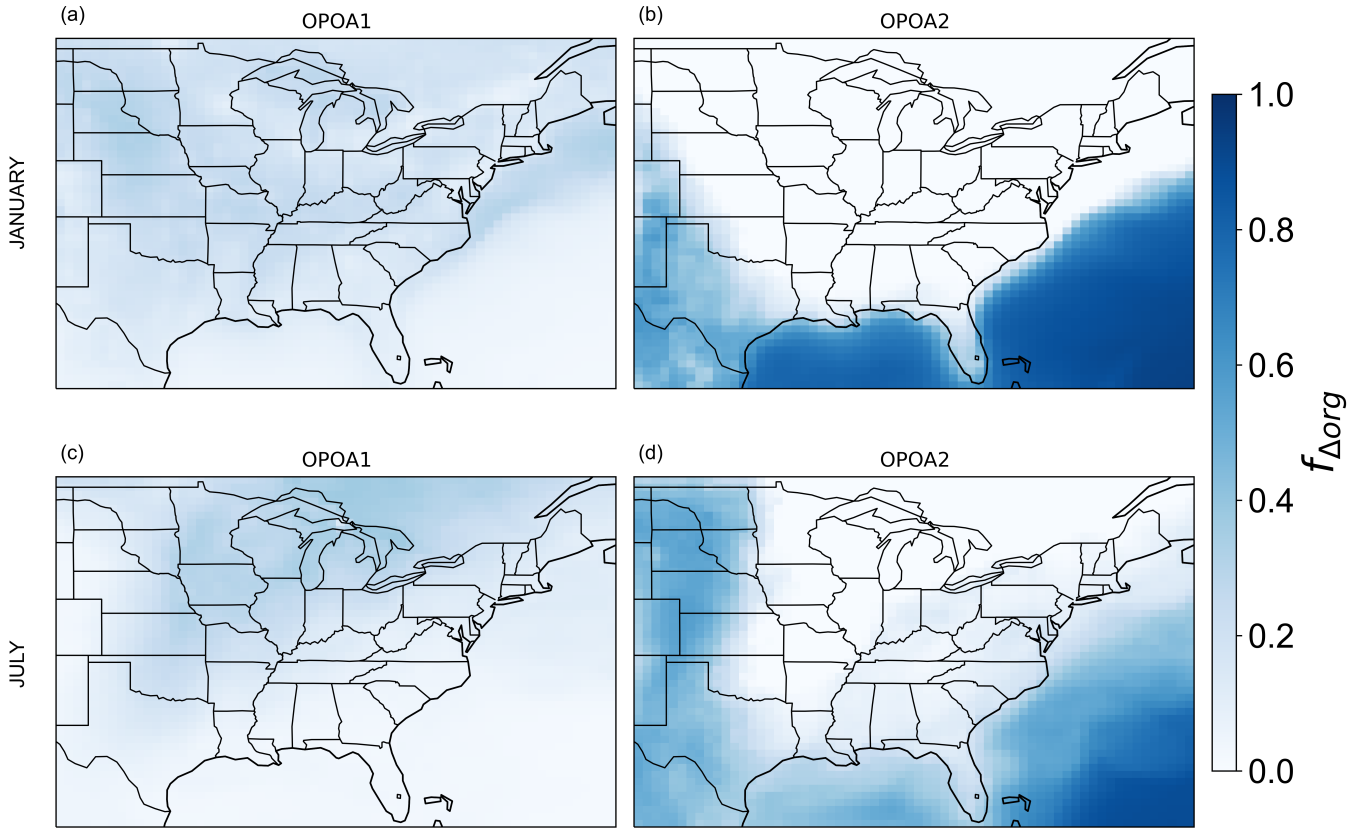

Figure S11. January 2019 (top panels) and July 2019 (bottom panels) monthly mean surface contribution of OA species from oxidized semivolatile organic compounds (OPOA) to the absolute difference in OA organic mass concentration, expressed as the organic mass concentration change fraction $f_{\Delta org}$. Panels **(a)** and **(c)** show the contribution of OPOA1 ($C_j^* = 16.46\ \mu g\,m^{-3}$). Panels **(b)** and **(d)** show the contribution of OPOA2 ($C_j^* = 0.2\ \mu g\,m^{-3}$).

where C_j^{OA} and ρ_j^{OA} are the OA organic mass concentration and density of the organic species j in the OA, respectively.

The density of the organic species j in the OA can be approximated using its elemental ratios (Kuwata et al., 2012):

$$\rho_j^{\mathrm{OA}} = \frac{12 + (\mathrm{H:C}_j) + 16(\mathrm{O:C}_j)}{7 + 5(\mathrm{H:C}_j) + 4.15(\mathrm{O:C}_j)}, \tag{S9}$$

where $\mathrm{H:C}_j$ and $\mathrm{H:C}_j$ are the hydrogen-to-carbon and oxygen-to-carbon elemental ratios of the organic species j, respectively.

Due to the absence of information about the value of $\mathrm{H:C}_j$ for organic compounds in the OA phase, the elemental ratio was estimated in GEOS-Chem by $\mathrm{H:C}_j \approx 2 - \mathrm{O:C}_j$, using a slope of -1 in a Van Krevelen diagram (H:C vs O:C), which is a common assumption (Heald et al., 2010).

In each grid cell of the GEOS-Chem model, the cumulative organic and water volumes and RH can then be used to estimate the hygroscopicity parameter of the OA according to Eq. (S5).

Table S1. Molecular properties of organic compounds with elemental oxygen-to-carbon ratios (O:C$_j$) decreased by 30 %.

Species [a]	Precursor	C_j^*[µg m^{-3}] [b,c,d]	M_j[g mol^{-1}] [e]	O:C$_j$
TSOA0	Terpenes	0.1	304.9	0.34
TSOA1	Terpenes	1.0	274.5	0.38
TSOA2	Terpenes	10.0	241.0	0.43
TSOA3	Terpenes	100.0	209.3	0.48
SOAGX	Isoprene	0.0 [f]	227.2	0.59
SOAIE	Isoprene	0.0 [f]	203.7	0.61
LVOCOA	Isoprene	0.0 [f]	180.9	0.63
ASOAN	Light aromatics & IVOC	0.0	270.9	0.49
ASOA1	Light aromatics & IVOC	1.0	240.7	0.53
ASOA2	Light aromatics & IVOC	10.0	212.0	0.57
ASOA3	Light aromatics & IVOC	100.0	180.9	0.63
POA1	Primary SVOCs	1646.0	241.7	0.13
POA2	Primary SVOCs	20.0	294.8	0.13
OPOA1	Oxidized SVOCs	16.5	217.8	0.52
OPOA2	Oxidized SVOCs	0.2	257.4	0.52

[a] All organic compounds are assumed to have the ketone functionality in terms of the characteristic group type adjustment of BAT when running the BAT-VBS model in GEOS-Chem.

[b] C_j^* values are calculated at a reference T of 298 K for the TSOA and ASOA species. C_j^* values are calculated at a reference T of 300 K for the POA and OPOA species.

[c] The enthalpy of vaporization normalized by the ideal gas constant used in GEOS-Chem is 5000 K.

[d] C_j^* values are assumed to be the same as in the GEOS-Chem simulation with unaltered O:C$_j$ values.

[e] M_j values increase as a result of decreasing O:C$_j$ values according to the molecular corridor relationship discussed in Sec. 2.1.

[f] Isoprene-derived species are assigned an C_j^* of 0 µg m^{-3} in order to reconcile the 1D VBS and Odum 2-product approaches of TSOA, ASOA, POA, and OPOA with the irreversible reactive uptake mechanism of ISOA.

Figure S15a shows the vertical profile of $\kappa_{org}^{\mathrm{OA}}$ from the first atmospheric level (0.058 km) up to an elevation of 2 km. The variation of $\kappa_{org}^{\mathrm{OA}}$ with elevation is affected by the composition of OA and RH at each vertical level. Due to its high mass fraction (Fig. S16c) and polarity (Table 2), the oxidized SVOCs species OPOA2 dominates the overall hygroscopicity of the OA within the entire 2 km layer. The vertical profile of the individual mass fractions of organic compounds (f_{org}) in the OA (with respect to the cumulative OA organic mass concentration) is shown in Fig. S16. The vertical profile of f_{org} for the different compound classes in GEOS-Chem is shown in S15b.

The BAT-VBS model does not need to calculate κ to estimate the hygroscopicity of OA and its associated water uptake. This exercise was only done to compare the predictions of the BAT-VBS model with the common assumption adopted in

Table S2. Molecular properties of organic compounds with elemental oxygen-to-carbon ratios (O:C$_j$) increased by 30 %.

Species [a]	Precursor	C_j^*[μg m^{-3}] [b,c,d]	M_j[g mol^{-1}] [e]	O:C$_j$
TSOA0	Terpenes	0.1	234.5	0.64
TSOA1	Terpenes	1.0	200.2	0.71
TSOA2	Terpenes	10.0	164.4	0.79
TSOA3	Terpenes	100.0	131.8	0.90
SOAGX	Isoprene	0.0 [f]	135.0	1.09
SOAIE	Isoprene	0.0 [f]	123.0	1.13
LVOCOA	Isoprene	0.0 [f]	111.0	1.17
ASOAN	Light aromatics & IVOC	0.0	168.9	0.91
ASOA1	Light aromatics & IVOC	1.0	139.5	0.99
ASOA2	Light aromatics & IVOC	10.0	123.0	1.07
ASOA3	Light aromatics & IVOC	100.0	111.0	1.17
POA1	Primary SVOCs	1646.0	223.3	0.25
POA2	Primary SVOCs	20.0	272.6	0.25
OPOA1	Oxidized SVOCs	16.5	126.4	0.97
OPOA2	Oxidized SVOCs	0.2	150.5	0.97

[a] All organic compounds are assumed to have the ketone functionality in terms of the characteristic group type adjustment of BAT when running the BAT-VBS model in GEOS-Chem.

[b] C_j^* values are calculated at a reference T of 298 K for the TSOA and ASOA species. C_j^* values are calculated at a reference T of 300 K for the POA and OPOA species.

[c] The enthalpy of vaporization normalized by the ideal gas constant used in GEOS-Chem is 5000 K.

[d] C_j^* values are assumed to be the same as in the GEOS-Chem simulation with unaltered O:C$_j$ values.

[e] M_j values decrease as a result of increasing O:C$_j$ values according to the molecular corridor relationship discussed in Sec. 2.1.

[f] Isoprene-derived species are assigned an C_j^* of 0 μg m^{-3} in order to reconcile the 1D VBS and Odum 2-product approaches of TSOA, ASOA, POA, and OPOA with the irreversible reactive uptake mechanism of ISOA.

large-scale 3D models to assign a constant κ value to characterize the water affinity of the OA (Pankow and Barsanti, 2009; Zhang et al., 2012; Pankow et al., 2015; Jathar et al., 2016; Pye et al., 2017; Kim et al., 2019). The outputs of the BAT-VBS model can be used to analyze the variation of κ over space and time. The aerosol impact on climate via aerosol–radiation and aerosol–radiation–cloud interactions are sensitive to the parameterized aerosol hygroscopicity and water uptake in large-scale 3D models (Rastak et al., 2017). While not the only source of uncertainty in climate models, using a constant κ to represent the water affinity of OA can lead to considerable errors when estimating the climate impact of aerosols.

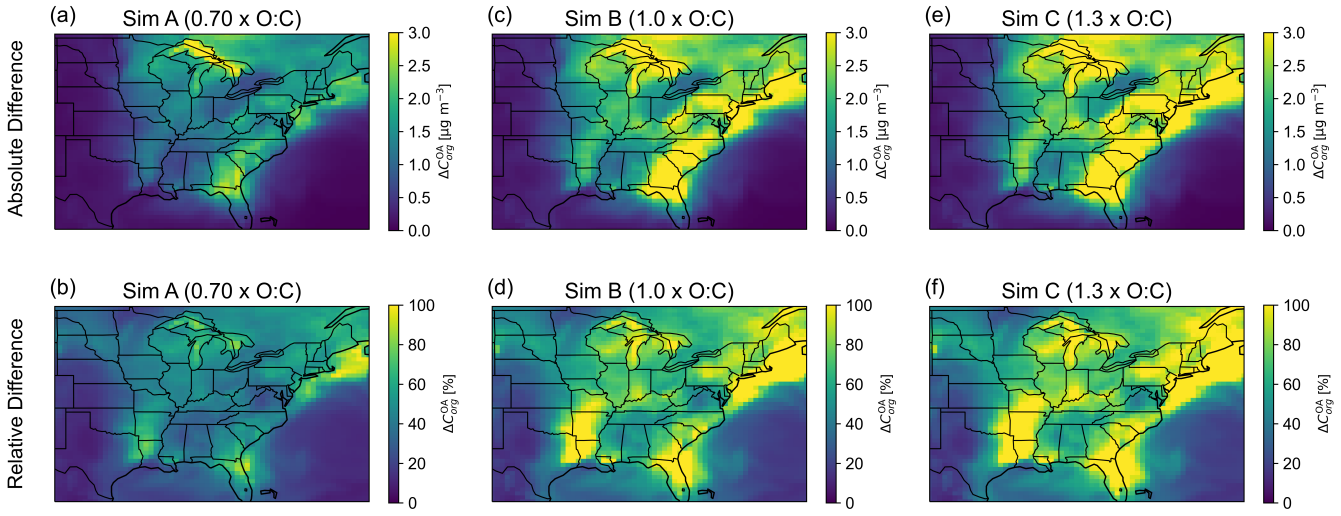

Figure S12. Weekly mean surface OA organic mass concentration enhancement (with respect to dry conditions) predicted by the introduced water-sensitive OA scheme (BAT-VBS model) for the first week of July 2019 using different reasonable O:C ranges. Panels **(a)** and **(b)** show the absolute and relative differences in weekly mean surface OA organic mass concentrations when O:C is decreased by 30 % (simulation A) with respect to the suggested values defined in Table 2. Panels **(c)** and **(d)** show the absolute and relative differences in weekly mean surface OA organic mass concentrations using the same molecular properties as defined in Table 2 (simulation B). Panels **(e)** and **(f)** show the absolute and relative differences in weekly mean surface OA organic mass concentrations when O:C is increased by 30 % (simulation C) with respect to the suggested values defined in Table 2. The surface level is the lowest atmospheric level of the GEOS-Chem model. The absolute and relative differences are calculated using the water-sensitive OA scheme (BAT-VBS model) at dry conditions as the reference ($C^{\mathrm{OA}}_{org,\mathrm{BAT-VBS}}$ (RH) - $C^{\mathrm{OA}}_{org,\mathrm{BAT-VBS}}$ (RH = 0 %)).

S9 Observations of Daily Mean $PM_{2.5}$ Mass Concentrations

The observed daily mean $PM_{2.5}$ mass concentrations shown in Fig. 7 were measured at monitoring sites located at specific geographical locations. Each panel displays the observations recorded at a specific point in latitude and longitude (see Table S3). We selected four monitoring sites for which the daily mean $PM_{2.5}$ data were available for every day of July 2019. We chose observation stations far enough from each other to compare our simulations with observations under different atmospheric conditions, emissions, and winds (Sec. 3.6). The air quality stations used are part of the U.S. Environmental Protection Agency's Air Quality System (AQS) monitoring network and repository. $PM_{2.5}$ mass concentration data were retrieved from the online-accessible repository without any further processing (U.S. Environmental Protection Agency, 2025).

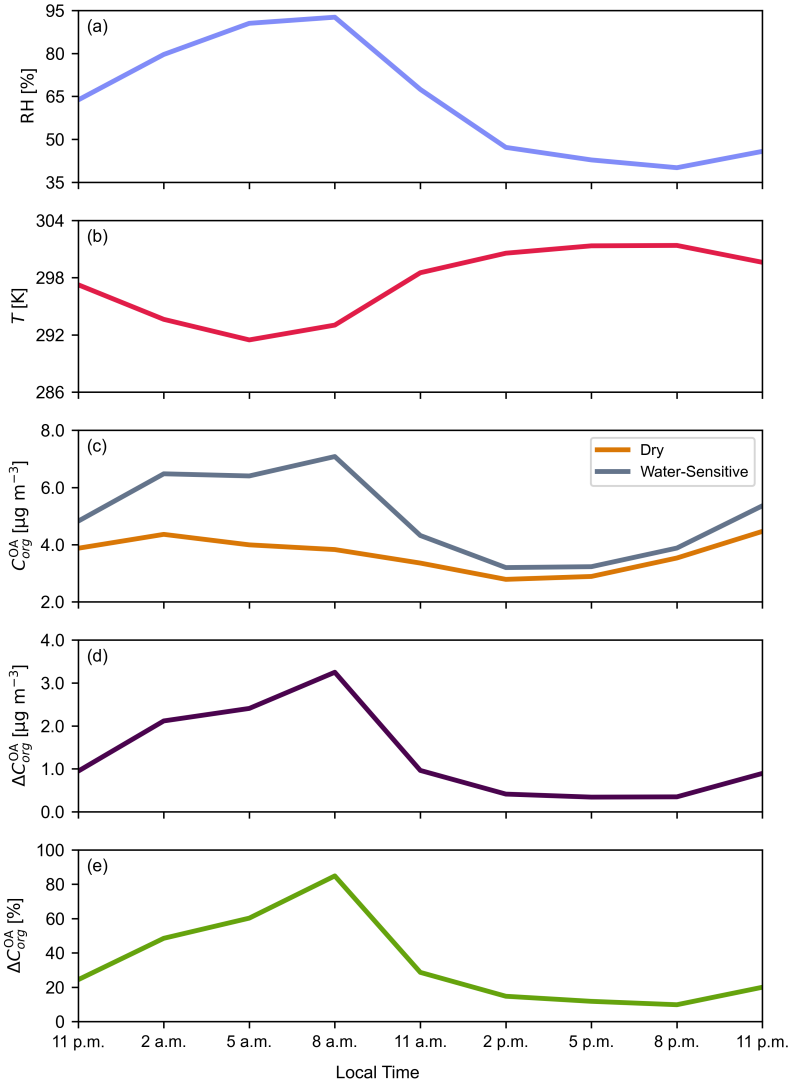

Figure S13. Time series of three-hourly values of surface RH, T, and OA properties predicted by the introduced water-sensitive OA scheme (BAT-VBS model) for Montreal, Canada, on July 3–4, 2019. The panels show: **(a)** the relative humidity, **(b)** the temperature, **(c)** the OA organic mass concentration, **(d)** the absolute difference in OA organic mass concentration, and **(e)** the relative difference in OA organic mass concentration. The absolute and relative differences are calculated using the water-sensitive OA scheme (BAT-VBS model) at dry conditions as the reference ($C^{\mathrm{OA}}_{org,\mathrm{BAT-VBS}}$ (RH) - $C^{\mathrm{OA}}_{org,\mathrm{BAT-VBS}}$ (RH = 0 %)).

S10 RH Threshold for the BAT-VBS model

The water-sensitive (introduced) OA scheme enhances the OA organic mass concentration with respect a dry OA scheme in any grid cell where RH is above 0 %, as explained in Sec. 3.2. In our simulations, described in Sec. 2.1, we used the

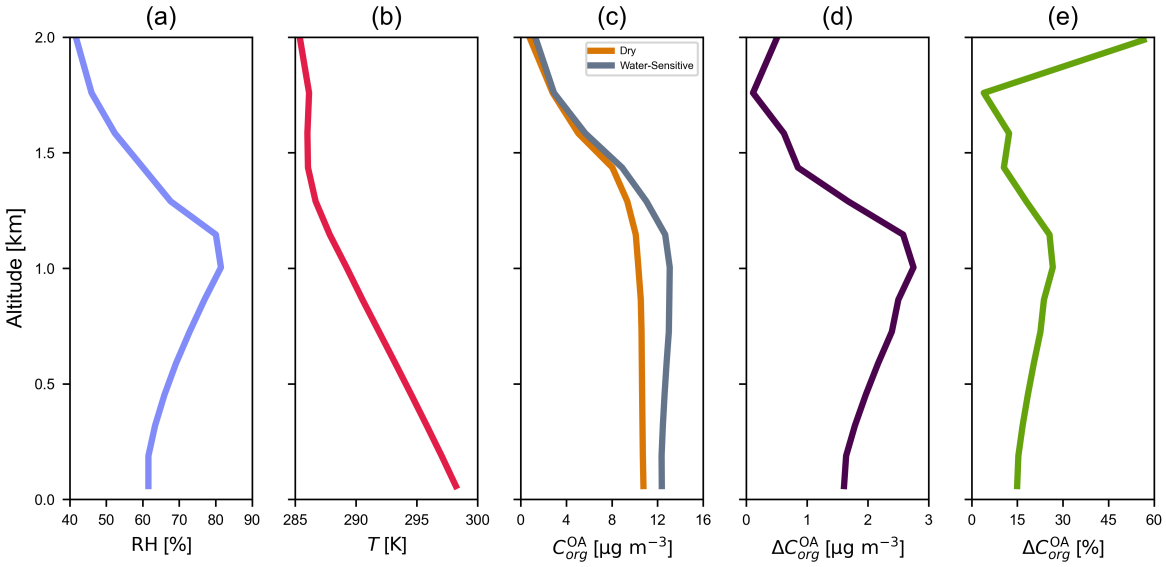

Figure S14. Vertical profile of surface RH, T, and OA properties predicted by the introduced water-sensitive OA scheme (BAT-VBS model) over Montreal, Canada, on July 6, 2019, at 5 p.m. local time. The panels show: **(a)** the relative humidity, **(b)** the temperature, **(c)** the OA organic mass concentration, **(d)** the absolute difference in OA organic mass concentration, and **(e)** the relative difference in OA organic mass concentration. The absolute and relative differences are calculated using the water-sensitive OA scheme (BAT-VBS model) at dry conditions as the reference ($C^{\mathrm{OA}}_{org,\mathrm{BAT-VBS}}$ (RH) - $C^{\mathrm{OA}}_{org,\mathrm{BAT-VBS}}$ (RH = 0 %)).

Table S3. Geographical locations of monitoring sites from which measured daily $PM_{2.5}$ data were obtained for the model–measurement comparison shown in Fig. 7. Data were retrieved from and processed by the U.S. Environmental Protection Agency (2025) Air Quality System.

Monitoring Station Number	Latitude (°)	Longitude (°)	U.S. State	County
1	32.79	-79.96	South Carolina	Charleston
2	37.26	-93.30	Missouri	Greene
3	30.46	-91.18	Louisiana	East Baton Rouge
4	40.50	-80.07	Pennsylvania	Allegheny

introduced water-sensitive OA scheme instead of GEOS-Chem's default OA scheme in all the grid cells of the GEOS-Chem model. It is possible, however, to reduce the computational costs associated with the introduced OA scheme by limiting the water-sensitive treatment to certain grid cells where RH is above a given threshold and using GEOS-Chem's default (dry) OA scheme elsewhere. In other words, the water-sensitive OA scheme could be reserved for grid cells where RH conditions lead to a significant enhancement in OA organic mass concentration with respect to the default (dry) OA scheme. The definition of

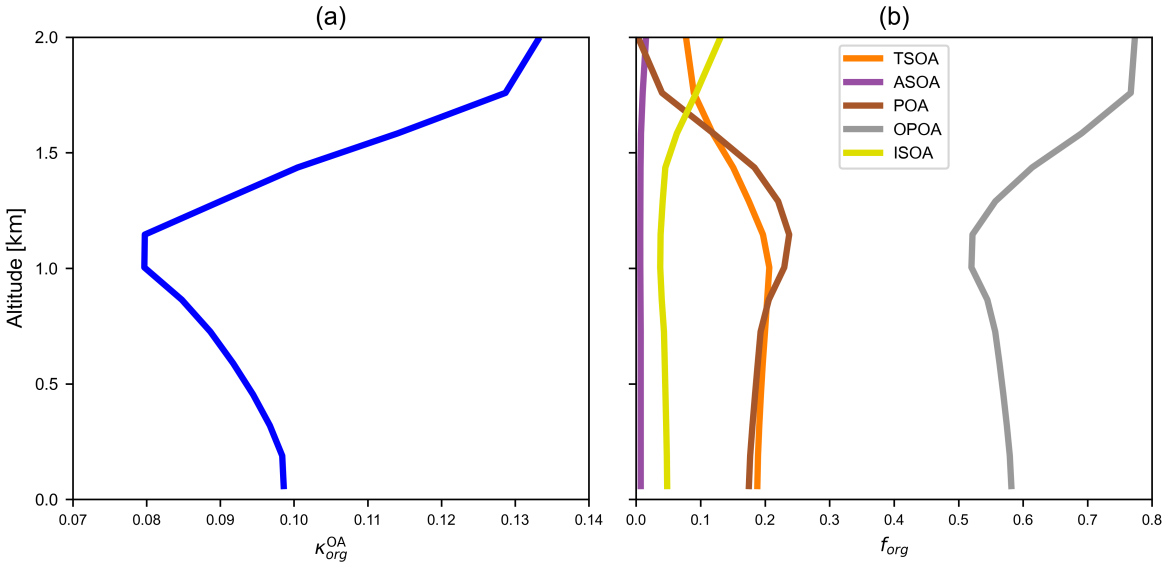

Figure S15. Vertical profile of OA properties predicted by the water-sensitive OA scheme (BAT-VBS model) over Montreal, Canada, on July 6, 2019 (5 p.m. local time). Panel **(a)** shows the OA hygroscopicity parameter. Panel **(b)** shows the contribution of OA compound classes to the OA organic mass concentration, expressed as the organic mass fraction f_{org}.

Table S4. Water-sensitive OA organic mass concentration enhancement associated with different mean RH conditions over North America

$\Delta C_{org}^{\mathrm{OA}}$ (%)	Mean RH threshold (%)	Frequency of RH values above the RH threshold (%)
10	5.0	47.4
20	9.6	45.3
30	13.5	43.8
40	16.2	42.8
50	18.2	42.1

a significant enhancement in OA organic mass concentration is subjective. For example, a GEOS-Chem user might decide that an OA organic mass concentration enhancement of $10\ \%$ or more is considered significant, in which case the BAT-VBS model would be used in all grid cells where RH $> 5\ \%$ and the default (dry) OA scheme elsewhere. Using the outputs of our July 2019 nested simulation, which considers the 72 vertical levels of the North American domain ($-140°$ to $-40°$ longitude and $10°$ to $70°$ latitude), we calculated the mean RH (threshold) value associated with different water-sensitive OA organic mass concentration enhancements ($\Delta C_{org}^{\mathrm{OA}}$) (Table S4). In addition, we calculated the frequency of grid cells where RH was greater than the threshold value. For example, $47.4\ \%$ of the grid cells had a RH value greater than $5\ \%$ in July 2019.

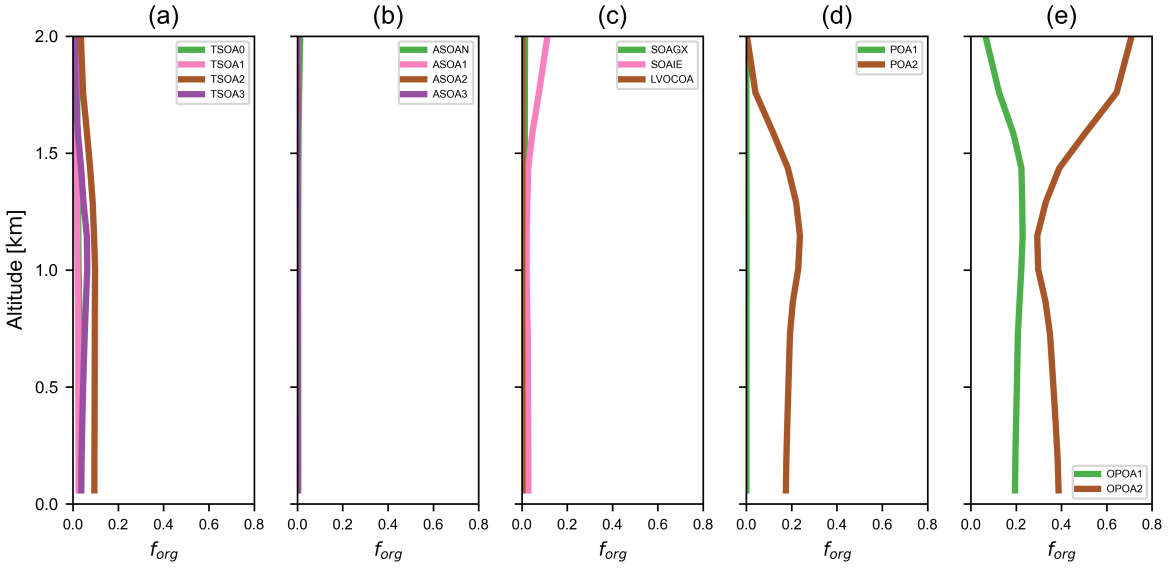

Figure S16. Vertical profile of OA properties predicted by the water-sensitive OA scheme (BAT-VBS model) over Montreal, Canada, on July 6, 2019 (5 p.m. local time). The contribution of OA species to the OA organic mass concentration is expressed as the organic mass fraction f_{org}. Panel **(a)** shows the contribution of OA species from terpenes (TSOA0, TSOA1, TSOA2, and TSOA3). Panel **(b)** shows the contribution of OA species from light aromatics & intermediate-volatility organic compounds (ASOAN, ASOA1, ASOA2, and ASOA3). Panel **(c)** shows the contribution of OA species from isoprene (SOAGX, SOAIE, and LVOCOA). Panel **(d)** shows the contribution of OA species from primary semivolatile organic compounds (POA1 and POA2). Panel **(e)** shows the contribution of OA species from oxidized semivolatile organic compounds (OPOA1 and OPOA2).

References

Chung, S. H. and Seinfeld, J. H.: Global distribution and climate forcing of carbonaceous aerosols, Journal of Geophysical Research: Atmospheres, 107, AAC 14–1–AAC 14–33, https://doi.org/https://doi.org/10.1029/2001JD001397, 2002.

Donahue, N. M., Robinson, A. L., Stanier, C. O., and Pandis, S. N.: Coupled Partitioning, Dilution, and Chemical Aging of Semivolatile Organics, Environmental Science & Technology, 40, 2635–2643, https://doi.org/10.1021/es052297c, 2006.

Gorkowski, K., Preston, T. C., and Zuend, A.: Relative-humidity-dependent organic aerosol thermodynamics via an efficient reduced-complexity model, Atmos. Chem. Phys., 19, 13 383–13 407, https://doi.org/10.5194/acp-19-13383-2019, 2019.

Heald, C. L., Kroll, J. H., Jimenez, J. L., Docherty, K. S., DeCarlo, P. F., Aiken, A. C., Chen, Q., Martin, S. T., Farmer, D. K., and Artaxo, P.: A simplified description of the evolution of organic aerosol composition in the atmosphere, Geophysical Research Letters, 37, https://doi.org/https://doi.org/10.1029/2010GL042737, 2010.

Jathar, S. H., Mahmud, A., Barsanti, K. C., Asher, W. E., Pankow, J. F., and Kleeman, M. J.: Water uptake by organic aerosol and its influence on gas/particle partitioning of secondary organic aerosol in the United States, Atmospheric Environment, 129, 142–154, https://doi.org/https://doi.org/10.1016/j.atmosenv.2016.01.001, 2016.

Kim, Y., Sartelet, K., and Couvidat, F.: Modeling the effect of non-ideality, dynamic mass transfer and viscosity on SOA formation in a 3-D air quality model, Atmos. Chem. Phys., 19, 1241–1261, https://doi.org/10.5194/acp-19-1241-2019, aCP, 2019.

Kuwata, M., Zorn, S. R., and Martin, S. T.: Using Elemental Ratios to Predict the Density of Organic Material Composed of Carbon, Hydrogen, and Oxygen, Environ. Sci. Technol., 46, 787–794, https://doi.org/10.1021/es202525q, 2012.

Marais, E. A., Jacob, D. J., Jimenez, J. L., Campuzano-Jost, P., Day, D. A., Hu, W., Krechmer, J., Zhu, L., Kim, P. S., Miller, C. C., Fisher, J. A., Travis, K., Yu, K., Hanisco, T. F., Wolfe, G. M., Arkinson, H. L., Pye, H. O. T., Froyd, K. D., Liao, J., and McNeill, V. F.: Aqueous-phase mechanism for secondary organic aerosol formation from isoprene: application to the southeast United States and co-benefit of SO_2 emission controls, Atmospheric Chemistry and Physics, 16, 1603–1618, https://doi.org/10.5194/acp-16-1603-2016, 2016.

Pankow, J. F.: An absorption model of the gas/aerosol partitioning involved in the formation of secondary organic aerosol, Atmospheric Environment, 28, 189–193, https://doi.org/https://doi.org/10.1016/1352-2310(94)90094-9, 1994.

Pankow, J. F.: Gas/particle partitioning of neutral and ionizing compounds to single and multi-phase aerosol particles. 1. Unified modeling framework, Atmospheric Environment, 37, 3323–3333, https://doi.org/https://doi.org/10.1016/S1352-2310(03)00346-7, 2003.

Pankow, J. F. and Barsanti, K. C.: The carbon number-polarity grid: A means to manage the complexity of the mix of organic compounds when modeling atmospheric organic particulate matter, Atmospheric Environment, 43, 2829–2835, https://doi.org/https://doi.org/10.1016/j.atmosenv.2008.12.050, 2009.

Pankow, J. F., Marks, M. C., Barsanti, K. C., Mahmud, A., Asher, W. E., Li, J., Ying, Q., Jathar, S. H., and Kleeman, M. J.: Molecular view modeling of atmospheric organic particulate matter: Incorporating molecular structure and co-condensation of water, Atmospheric Environment, 122, 400–408, https://doi.org/https://doi.org/10.1016/j.atmosenv.2015.10.001, 2015.

Petters, M. D. and Kreidenweis, S. M.: A single parameter representation of hygroscopic growth and cloud condensation nucleus activity, Atmos. Chem. Phys., 7, 1961–1971, https://doi.org/10.5194/acp-7-1961-2007, 2007.

Pye, H. O. T., Chan, A. W. H., Barkley, M. P., and Seinfeld, J. H.: Global modeling of organic aerosol: the importance of reactive nitrogen (NO_x and NO_3), Atmos. Chem. Phys., 10, 11 261–11 276, https://doi.org/10.5194/acp-10-11261-2010, 2010.

Pye, H. O. T., Murphy, B. N., Xu, L., Ng, N. L., Carlton, A. G., Guo, H., Weber, R., Vasilakos, P., Appel, K. W., Budisulistiorini, S. H., Surratt, J. D., Nenes, A., Hu, W., Jimenez, J. L., Isaacman-VanWertz, G., Misztal, P. K., and Goldstein, A. H.: On the implications of aerosol liquid water and phase separation for organic aerosol mass, Atmos. Chem. Phys., 17, 343–369, https://doi.org/10.5194/acp-17-343-2017, 2017.

Rastak, N., Pajunoja, A., Acosta Navarro, J. C., Ma, J., Song, M., Partridge, D. G., Kirkevåg, A., Leong, Y., Hu, W. W., Taylor, N. F., Lambe, A., Cerully, K., Bougiatioti, A., Liu, P., Krejci, R., Petäjä, T., Percival, C., Davidovits, P., Worsnop, D. R., Ekman, A. M. L., Nenes, A., Martin, S., Jimenez, J. L., Collins, D. R., Topping, D. O., Bertram, A. K., Zuend, A., Virtanen, A., and Riipinen, I.: Microphysical explanation of the RH-dependent water affinity of biogenic organic aerosol and its importance for climate, Geophys Res Lett, 44, 5167–5177, https://doi.org/10.1002/2017gl073056, 2017.

Serrano Damha, C., Cummings, B. E., Schervish, M., Shiraiwa, M., Waring, M. S., and Zuend, A.: Capturing the Relative-Humidity-Sensitive Gas–Particle Partitioning of Organic Aerosols in a 2D Volatility Basis Set, Geophysical Research Letters, 51, e2023GL106 095, https://doi.org/https://doi.org/10.1029/2023GL106095, 2024.

U.S. Environmental Protection Agency: Air Quality System Data Mart, [internet database] available at https://www.epa.gov/outdoor-air-quality-data., last access: 6 January 2025, 2025.

Zhang, K., O'Donnell, D., Kazil, J., Stier, P., Kinne, S., Lohmann, U., Ferrachat, S., Croft, B., Quaas, J., Wan, H., Rast, S., and Feichter, J.: The global aerosol-climate model ECHAM-HAM, version 2: sensitivity to improvements in process representations, Atmos. Chem. Phys., 12, 8911–8949, https://doi.org/10.5194/acp-12-8911-2012, aCP, 2012.

Zuend, A., Marcolli, C., Peter, T., and Seinfeld, J. H.: Computation of liquid-liquid equilibria and phase stabilities: implications for RH-dependent gas/particle partitioning of organic-inorganic aerosols, Atmos. Chem. Phys., 10, 7795–7820, https://doi.org/10.5194/acp-10-7795-2010, 2010.